XVI International Conference on Computational Plasticity. Fundamentals and Applications
COMPLAS 2021
E. Oñate, D. Peric, M. Chiumenti and Eduardo de Souza Neto (Eds)

FRACTURE MECHANICS EVALUATION OF V-BENDING DIE WITH A HOLE USING PARAMETRIC ANALYSIS SYSTEM WITH COUPLING-MATRIX-FREE ITERATIVE S-VERSION FEM

HIROKI SUWA[*] AND YASUNORI YUSA[†]

[*] The University of Electro-Communications
1-5-1, Chofugaoka, Chofu, Tokyo 182-8585, Japan
e-mail: hiroki.suwa@uec.ac.jp

[†] The University of Electro-Communications
1-5-1, Chofugaoka, Chofu, Tokyo 182-8585, Japan
email: y.yusa@uec.ac.jp, www.yusa.lab.uec.ac.jp

Key words: S-version FEM, Parametric study, Fracture mechanics

Abstract. Parametric studies of structures with holes using the conventional finite element method (FEM) have difficulties with regard to remeshing. To avoid this problem, a coupling-matrix-free iterative s-version FEM can create separate meshes for the whole analysis domain and the vicinity of a hole. In this study, we proposed a parametric analysis system to analyze a die with a hole for the V-bending process, and we evaluated the results in terms of fracture mechanics. We considered both brittle fracture and fatigue fracture modes. We evaluated fatigue fracture by maximum principal stress and brittle fracture by stress intensity factors. In the present parametric analysis, we evaluated a V-bending die with a hole by simply moving the center coordinates of the local mesh. Thus, this system makes it possible to perform a parametric analysis automatically with a single command. As a result of the parametric analysis with various hole coordinates, we found coordinates that reduced both the maximum principal stress at the V-groove bottom and the stress intensity factors at the deepest part of a crack.

1 INTRODUCTION

In the process of bending metal plates into a V shape (V-bending), occasionally the die breaks under extreme stress. Moreover, sometimes press operators are injured by pieces of a crushed die. Therefore, it is necessary to avoid these accidents by designing a V-bending die that is more difficult to break.

According to previous research [1], the tensile stress in a V-bending die with a hole is smaller than that in one without a hole. Using the conventional finite element method (FEM), every time the hole characteristics are changed, remeshing is required. Thus, in this study, we used coupling-matrix-free iterative s-version FEM [2], which is a modification of the s-version FEM [3]. In this method, the mesh for the whole analysis domain and the mesh in the vicinity of the hole are created separately, and so it is not necessary to perform remeshing in a parametric study of the hole coordinates.

The purpose of the present study was to develop a method to easily perform parametric

analyses of hole coordinates. Therefore, a V-bending die with a hole was subjected to a parametric study of its coordinates. We assumed failure modes of fatigue fracture and brittle fracture. We used maximum principal stresses to evaluate a die by fatigue fracture. Regarding brittle fracture, we used a mesh with a crack to assess stress intensity factors in the deepest part of the crack.

2 COMPUTATIONAL METHOD

2.1 Coupling-matrix-free iterative s-version FEM [2]

According to the literature [2], in the coupling-matrix-free iterative s-version FEM, a local mesh and a global mesh can be configured as shown in Figure 1. A local domain Ω^L, a global mesh domain Ω^G, a global−local interface Γ^{GL}, a geometric boundary condition Γ_u, and a mechanical boundary condition Γ_t are defined. Here, the displacement $\boldsymbol{u}$ and the virtual displacement $\boldsymbol{\delta u}$ are calculated using Eq. (1) and Eq. (2), respectively.

$$\boldsymbol{u} = \begin{cases} \boldsymbol{u}^G & in\ \Omega^G \setminus \Omega^L \\ \boldsymbol{u}^G + \boldsymbol{u}^L & in\ \Omega^L \end{cases}, \tag{1}$$

$$\boldsymbol{\delta u} = \begin{cases} \boldsymbol{\delta u}^G & in\ \Omega^G \setminus \Omega^L \\ \boldsymbol{\delta u}^G + \boldsymbol{\delta u}^L & in\ \Omega^L \end{cases}. \tag{2}$$

On Γ^{GL}, $\boldsymbol{u}$ and $\boldsymbol{\delta u}$ satisfy Eq. (3),

$$\boldsymbol{u}^L = \boldsymbol{\delta u}^L = 0 \quad on\ \Gamma^{GL}. \tag{3}$$

The principle of visual work is given as

$$\int_\Omega \boldsymbol{\delta\varepsilon}^T \boldsymbol{D\varepsilon} d\Omega = \int_{\Gamma_t} \boldsymbol{\delta u}^T \boldsymbol{t} d\Gamma + \int_\Omega \boldsymbol{\delta u}^T \boldsymbol{b} d\Omega, \tag{4}$$

where a strain $\boldsymbol{\varepsilon}$, traction $\boldsymbol{t}$, and body force $\boldsymbol{b}$ are assumed.

Eq. (1), Eq. (2), and Eq. (4) are used to derive Eq. (5) and Eq. (6), where $\boldsymbol{D}$ is the elasticity matrix and $\boldsymbol{\sigma}$ is a local stress vector.

$$\int_{\Omega^G} \boldsymbol{\delta\varepsilon}^{G^T} \boldsymbol{D\varepsilon}^G d\Omega = -\int_{\Omega^L} \boldsymbol{\delta\varepsilon}^{G^T} \boldsymbol{\sigma}^L d\Omega + \int_{\Gamma_t^G} \boldsymbol{\delta u}^{G^T} \boldsymbol{t} d\Gamma + \int_{\Omega^G} \boldsymbol{\delta u}^{G^T} \boldsymbol{b} d\Omega, \tag{5}$$

$$\int_{\Omega^L} \boldsymbol{\delta\varepsilon}^{L^T} \boldsymbol{D\varepsilon}^L d\Omega = -\int_{\Omega^L} \boldsymbol{\delta\varepsilon}^{L^T} \boldsymbol{\sigma}^G d\Omega + \int_{\Gamma_t^L} \boldsymbol{\delta u}^{L^T} \boldsymbol{t} d\Gamma + \int_{\Omega^L} \boldsymbol{\delta u}^{L^T} \boldsymbol{b} d\Omega, \tag{6}$$

By discretizing and rearranging Eq. (5) and Eq. (6), the following equations are obtained:

$$\boldsymbol{K}^G \bar{u}^G = -\int_{\Omega^L} \boldsymbol{B}^{G^T} \bar{\boldsymbol{\sigma}}^L d\Omega + \boldsymbol{f}^G, \tag{7}$$

$$\boldsymbol{K}^L \bar{\boldsymbol{u}}^L = -\int_{\Omega^G} \boldsymbol{B}^{L^T} \bar{\boldsymbol{\sigma}}^G d\Omega + \boldsymbol{f}^L, \tag{8}$$

where a displacementstrain–matrix $\boldsymbol{B}$ is assumed and the stiffness matrix $\boldsymbol{K}$ and external force vector $\boldsymbol{f}$ are expressed as Eq. (9) to Eq. (12),

$$\boldsymbol{K}^G = \int_{\Omega^G} \boldsymbol{B}^{G^T} \boldsymbol{D} \boldsymbol{B}^G d\Omega, \tag{9}$$

$$\boldsymbol{K}^L = \int_{\Omega^L} \boldsymbol{B}^{L^T} \boldsymbol{D} \boldsymbol{B}^L d\Omega, \tag{10}$$

$$\boldsymbol{f}^G = \int_{\Gamma_t^G} \boldsymbol{N}^{G^T} \boldsymbol{t} d\Gamma + \int_{\Omega^G} \boldsymbol{N}^{G^T} \boldsymbol{b} d\Omega, \tag{11}$$

$$\boldsymbol{f}^L = \int_{\Gamma_t^L} \boldsymbol{N}^{L^T} \boldsymbol{t} d\Gamma + \int_{\Omega^L} \boldsymbol{N}^{L^T} \boldsymbol{b} d\Omega, \tag{12}$$

where $\boldsymbol{N}$ is a shape function.

In this method, the calculations are reiterated using Eq. (7) and Eq. (8). First, $\overline{\boldsymbol{\sigma}}^G$ is calculated by the FEM using only the global mesh. The resulting stress is transferred from the global mesh to the local mesh, and $\overline{\boldsymbol{\sigma}}^L$ is calculated for the local mesh. These calculations are repeated until they converge to a solusion. Here, we use the conditions of transferring stress referred to "scheme 2" in Ref. [2]. We use the nearest-neighbor interpolation as a way to transfer $\overline{\boldsymbol{\sigma}}^G$ and perform interpolation by the local-least squares method as a way to transfer $\overline{\boldsymbol{\sigma}}^L$. The sampling area of the local-least squares method matches one of the global elements. When these calculations are repeated, equilibria of internal forces and external forces are computed as relative residuals. When the relative residuals are less than a threshold value, the iterative calculation is finished. The equilibrium forces during iteration k-th are used for the following criterion formula with ε as threshold.

$$\frac{\left\| \begin{Bmatrix} \boldsymbol{f}^G + \boldsymbol{K}^G \overline{\boldsymbol{u}}^{G(k+1)} - \int_{\Omega^L} \boldsymbol{B}^{G^T} \overline{\boldsymbol{\sigma}}^{L(k+1)} d\Omega \\ \boldsymbol{f}^L + \boldsymbol{K}^L \overline{\boldsymbol{u}}^{L(k+1)} - \int_{\Omega^L} \boldsymbol{B}^{L^T} \overline{\boldsymbol{\sigma}}^{G(k+1)} d\Omega \end{Bmatrix} \right\|}{\left\| \begin{Bmatrix} \boldsymbol{f}^G \\ \boldsymbol{f}^L \end{Bmatrix} \right\|} \leq \varepsilon, \tag{13}$$

The block Gauss-Seidel method with Aitken acceleration [4] is used for iteration.

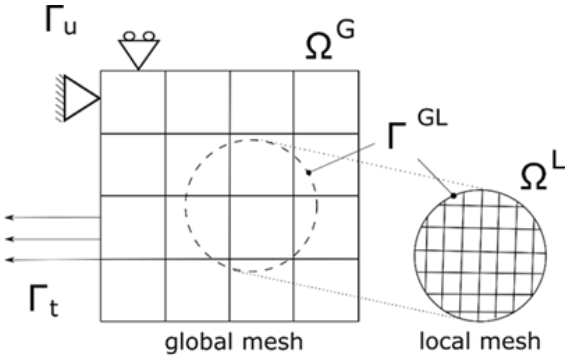

Figure 1: Domains and boundary conditions for coupling-matrix-free iterative s-FEM

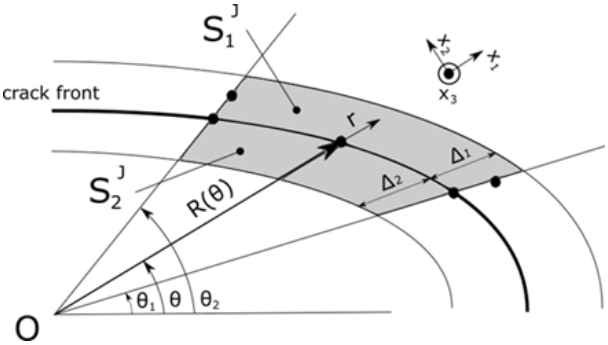

Figure 2: Example of elements near a crack

2.2 Calculation method for stress intensity factor [5]

We used a method proposed by Okada et al. [5] to calculate the stress intensity factors. The

energy release rates are computed by the virtual crack closure-integral method [6]. Figure 2 shows the elements of the crack surface for which energy release rates are calculated. We assumed that the widths of elements for calculation and the width of elements near calculated elements have the same value ($\Delta_1 = \Delta_2 = \Delta$). The failure mode in this study is mode I, so the following equations are applied under mode I. The deepest part of the crack is subjected to the plane strain condition.

To use Eq. (14) [6], the energy release rate G_{I} in an element with an area S_1^J is determined. Then, Young's modulus E, Poisson's ratio ν, the stress intensity factor K_{I}, the normal stress at the crack surface σ_{33}, and the vertical displacement of the crack surface v_3 are assumed. In mode I, Eq. (14) and Eq. (15) hold.

$$E' = E/(1-\nu^2), \tag{14}$$

$$G_{\mathrm{I}} = \frac{1}{2[S_1^J - \frac{1}{4}(S_1^J - S_2^J)]} \int_{S_1^J} \sigma_{33}(\boldsymbol{r}) v_3(\Delta - \boldsymbol{r}) dS_1^J. \tag{15}$$

Based on Eq. (15), Eq. (16) is derived as

$$G_{\mathrm{I}} = \frac{1}{2[S_1^J - \frac{1}{4}(S_1^J - S_2^J)]} \sum_{I=1}^{5} \bar{C}^I v_3^I P_3^I. \tag{16}$$

From Eq. (16), the energy release rate depends on the reaction force and displacement for each node.

As above, the energy release rate is calculated. From Ref. [7], Eq. (17) holds.

$$K_{\mathrm{I}} = \sqrt{\frac{E}{(1-\nu^2)} G_{\mathrm{I}}}. \tag{17}$$

The energy release rates that are computed, and Eq. (17) is used to derive the stress intensity factors.

2.3 Parametric analysis

In this study, we analyzed a V-bending die and used the central coordinates of a hole as parameters in this analysis. With the coupling-matrix-free iterative s-version FEM, hole coordinates are not fixed after meshes are created. To use this property, we created a script to conduct many analyses of various coordinates of a hole at once. Before we execute the script, we must first specify the central coordinates of the hole.

We conducted an analysis for holes with 336 different positions specified by the hole center coordinates.

3 ANALYSIS OF V-BENDING DIE

3.1 Analysis conditions

We used a die with a V-groove width of 10 mm made by AMADA CO., LTD. [8]. The metal material of the die was steel plate cold commercial (SPCC) with a Young's modulus of 206 GPa and Poisson's ratio of 0.3. Figure 3 shows the dimensions of the die. The global mesh size

was 0.5 mm, and its thickness was 5 mm. The shape of the local mesh was an ellipse with a major hole axis length of 1 mm, and a minor axis length of 0.5 mm. The inclination of the ellipse was 47° from the horizontal plane. The major axis of the local mesh was 2 mm long, and the minor axis was 1 mm long. Figure 5 shows the global and local meshes. We defined the V-bending die without a crack as global mesh 1, and the die with a crack as global mesh 2. The number of elements and nodes in each mesh are given in Table. 1.

We expected that most die failures are due to a crack in the V-groove bottom. Thus, we made a crack 0 mm thick in this location. The crack spacing was 10 mm, and its radius was 0.5 mm. According to Eq. (18) [7], which represents the stress state near a two-dimensional penetrating crack under uniform tensile stress, if the tensile stress σ_0 is 1 MPa, the stress 5 mm away from the center of the crack is 1.01 MPa. We considered this value as sufficiently small and set a crack spacing of 10 mm in this study.

$$\sigma = \frac{\sigma_0 x}{\sqrt{x^2 - a^2}} \tag{18}$$

The shape of an actual crack in a V-bending die is unknown. Therefore, we assume a semicircular shape for the crack. The size of the front of the crack Δ was about 0.014 mm. We used the 8-point Gaussian quadrature for the integration on elements.

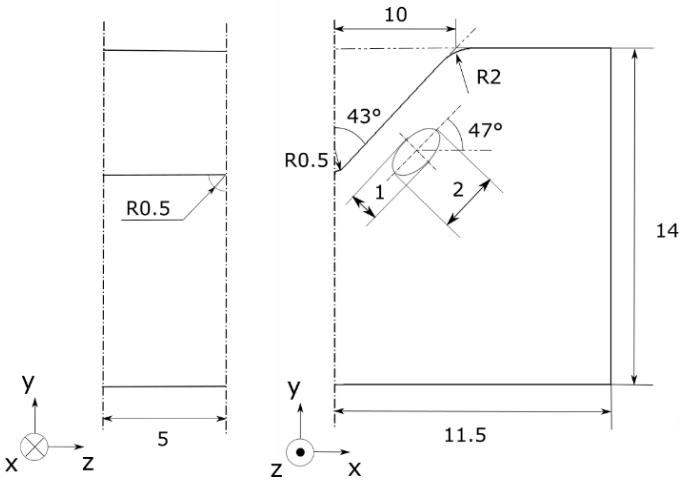

Figure 3: Size of V-bending die (Unit: mm)

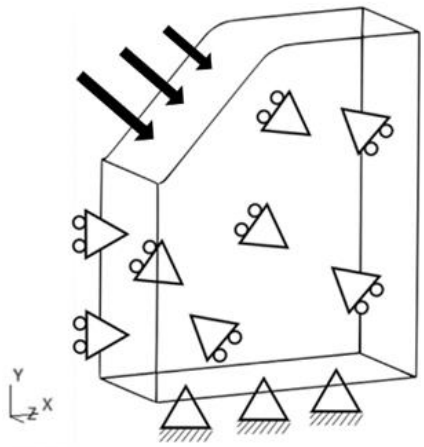

Figure 4: Boundary conditions

Table 1: Number of elements and nodes

Mesh	Elements	Nodes
Global mesh 1	600	1,300
Global mesh 2	5,295	6,590
Local mesh	46,256	50,400

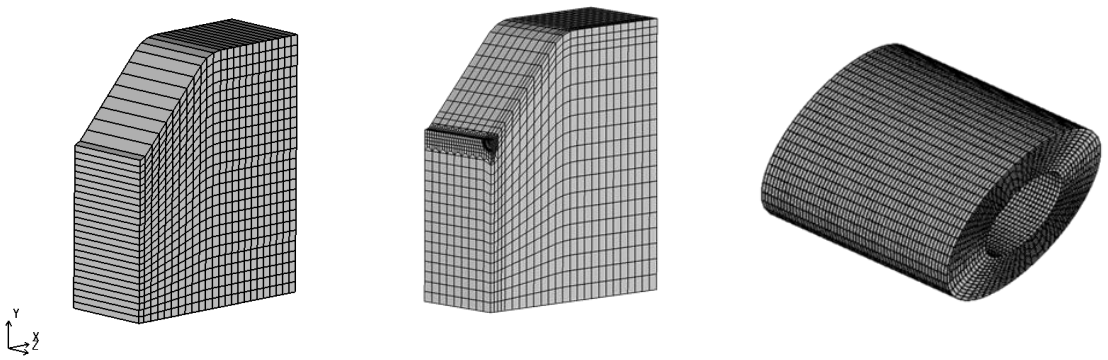

Figure 5: Global mesh 1 (no crack), global mesh 2 (with crack), and local mesh (hole)

Next, we conformed the model to the coordinate system and boundary conditions in Figure 4. We considered the length of the V-bending die in the z direction to be infinity and we regarded the surface of the V-groove as symmetric in the x direction, giving symmetric boundary conditions to each suitable surface. The bottom of a V-bending die is fixed during use, so clamped conditions were applied to the bottom of the V-bending die.

We used the results from process simulation of a V-bending die from the Kuboki Laboratory (University of Electro-Communications) [9] as the mechanical boundary conditions. In this simulation, the punch was a rigid body, the punch load was 0.1 tonf/mm, and the die made of steel with a Young's modulus of 205.8 GPa. The work-piece was a 1.6 mm thick SPCC plate.

The contact tractions shown in Figure 6 and Figure 7 were used as mechanical boundary conditions. In Figure 6, the horizontal axis is the x coordinate, and the vertical axis is traction in the x direction. In Figure 7, the horizontal axis is the x coordinate, and the vertical axis is traction in the -y direction. These values were used to assume value at the center of an element is the same as the traction at the surface. Thus, we approximated a constant traction on each element.

To use the traction described above, the first term on the right hand of the Eq. (11) is calculated.

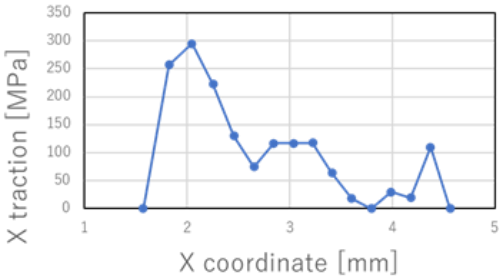

Figure 6: Mechanical boundary conditions in x direction

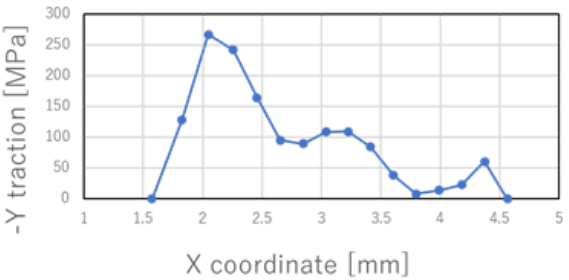

Figure 7: Mechanical boundary conditions in y direction

3.2 Results of analysis of maximum principal stress

This section describes how the global mesh without a crack was used to evaluate maximum

principal stress. Figures 8 and Figure 9 show the distributions of the maximum principal stress without a hole and with a hole, respectively. Note that the smallest maximum principal stress in Figure 9 is located at the V-groove bottom in the parametric analyses. The values of the maximum principal stress at the V-groove bottom using dies with and without a hole are 283 and 208 MPa, respectively. The central coordinates of the smallest maximum principal stress are (1.75, 9). The maximum principal stress decreased by 26.5% due to this hole.

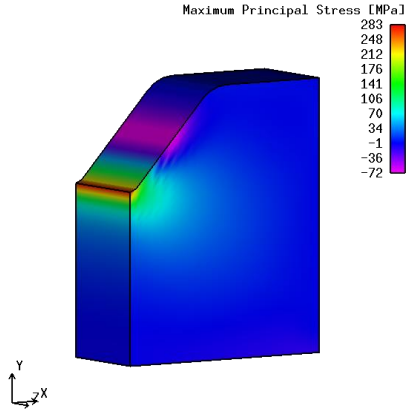

Figure 8: Maximum principal stress (without hole)

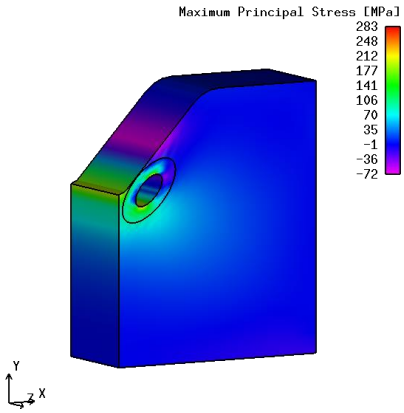

Figure 9: Maximum principal stress (with hole)

Figure 10 shows the distribution of maximum principal stress from the results of 336 parametric analyses. The horizontal and vertical axes are the coordinates of the center of the hole, and the maximum principal stress corresponding to each coordinate is given in each box with color-coding. The box of the value of the maximum principal stress without the hole, 283 MPa is yellow. The smaller the value in each box is than 283 MPa, the redder the box is, and the bigger, the greener.

y coordinate [mm]

	1.75	2.25	2.75	3.25	3.75	4.25	4.75	5.25	5.75	6.25	6.75	7.25	7.75	8.25	8.75	9.25	9.75
12							286	285	285	284	284	284	283	283	283	283	283
11.5						288	288	287	286	285	285	285	284	284	283	283	283
11					291	292	290	289	288	286	285	285	285	284	284	283	283
10.5				286	294	295	291	291	290	288	286	285	285	284	284	284	283
10			267	288	295	296	293	294	290	288	287	286	286	285	284	284	284
9.5		237	275	292	298	298	294	295	291	289	288	287	286	285	285	284	284
9	208	259	285	297	300	300	296	296	293	290	289	288	287	286	285	285	284
8.5	273	282	298	303	302	300	297	297	294	292	289	288	287	286	286	285	285
8	296	299	301	304	302	297	296	294	294	293	292	290	288	287	286	286	285
7.5	306	300	300	301	300	295	297	293	293	292	291	290	289	288	287	286	286
7	305	300	297	297	298	293	295	292	291	290	290	290	289	288	287	287	286
6.5	300	297	293	295	295	290	294	291	290	289	289	289	290	289	288	288	287
6	293	293	290	292	290	289	291	290	289	289	288	288	288	288	289	288	288
5.5	289	289	288	288	289	288	288	288	288	288	288	288	287	287	287	288	288
5	286	285	286	286	287	286	286	287	287	287	287	288	287	287	287	287	287
4.5	284	284	284	284	285	285	285	285	286	286	286	287	287	287	287	287	288
4	282	283	282	283	283	284	284	285	285	286	286	286	287	287	287	288	288
3.5	282	282	282	282	282	283	283	284	285	285	286	286	286	287	288	289	289
3	281	282	281	282	282	283	283	283	284	285	285	286	286	287	287	288	289
2.5	281	281	281	281	282	282	282	283	283	284	285	285	286	287	287	288	289
2	281	281	281	281	282	282	282	283	283	284	284	285	286	287	288	289	289

x coordinate [mm]

Figure 10: Distribution of maximum principal stress (MPa)

3.3 Results of the analysis of stress intensity factors

This section describes how we used the global mesh with a crack to evaluate the stress intensity factors. First, we used the conventional FEM to compare V-bending dies with and without a hole. Figure 11 shows the results for stress intensity factors near a crack in the V-bending die without a hole. The horizontal axis is the angle at each point along a semicircular crack, and the vertical axis is the stress intensity factor. In this study, we used the deepest part of the crack ($\theta = 90°$) as an evaluation index to make a comparison. The stress intensity factor for the deepest part of the crack is 4.74 MPa$\sqrt{\text{m}}$ in a V-bending die without a hole.

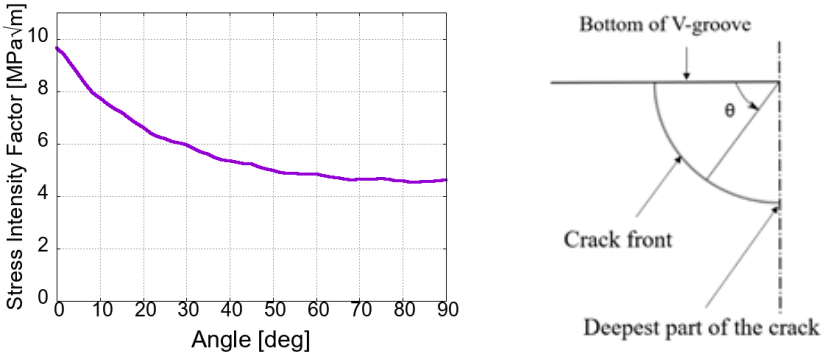

Figure 11: Stress intensity factor of V-bending die without a hole

Figure 12 shows the results of a parametric analysis for 336 different hole positions. In the figure, the horizontal and vertical axes are the coordinates of the center of the hole, and the stress intensity factors corresponding to each coordinate are given in each box with color coding. The box of the value of the stress intensity factor without the hole, 4.74 MPa$\sqrt{\text{m}}$ is yellow. The smaller the value in each box is than 4.74 MPa$\sqrt{\text{m}}$, the redder the box is, and the bigger, the greener.

From the results, the stress intensity factor for the central coordinates (1.75, 9) has the smallest value of about 3.39 MPa$\sqrt{\text{m}}$. The stress intensity factor at the deepest part of the crack with the central coordinates (1.75, 7) has the largest value of about 4.91 MPa$\sqrt{\text{m}}$. Figure 13 shows the residual history over time. The horizontal axis is the iteration step k, and the vertical axis is the right-hand side of Eq. (19). In this analysis, the residual after 17 iterations was lower than the threshold, $\varepsilon = 10^{-3}$.

y coordinate [mm]	1.75	2.25	2.75	3.25	3.75	4.25	4.75	5.25	5.75	6.25	6.75	7.25	7.75	8.25	8.75	9.25	9.75
12							4.67	4.67	4.66	4.66	4.65	4.64	4.64	4.64	4.63	4.63	4.63
11.5						4.69	4.70	4.69	4.68	4.67	4.66	4.65	4.64	4.64	4.64	4.63	4.63
11					4.70	4.74	4.71	4.70	4.69	4.68	4.67	4.66	4.65	4.65	4.64	4.64	4.63
10.5				4.60	4.70	4.71	4.73	4.74	4.70	4.70	4.69	4.68	4.67	4.66	4.65	4.64	4.64
10			4.35	4.54	4.70	4.69	4.78	4.71	4.72	4.70	4.70	4.68	4.67	4.66	4.66	4.65	4.64
9.5		4.01	4.25	4.52	4.67	4.76	4.73	4.76	4.72	4.72	4.70	4.69	4.68	4.67	4.66	4.65	4.65
9	3.39	3.92	4.30	4.55	4.70	4.74	4.73	4.75	4.75	4.72	4.71	4.70	4.68	4.67	4.67	4.66	4.65
8.5	3.48	4.11	4.49	4.64	4.71	4.70	4.77	4.75	4.74	4.73	4.72	4.71	4.69	4.68	4.67	4.67	4.66
8	4.33	4.52	4.69	4.72	4.73	4.83	4.74	4.75	4.74	4.73	4.73	4.72	4.70	4.69	4.68	4.67	4.67
7.5	4.80	4.74	4.77	4.74	4.76	4.77	4.80	4.73	4.74	4.73	4.72	4.71	4.70	4.69	4.68	4.68	4.67
7	4.91	4.82	4.76	4.77	4.77	4.73	4.75	4.74	4.74	4.72	4.71	4.71	4.70	4.69	4.68	4.68	4.67
6.5	4.88	4.84	4.79	4.79	4.76	4.76	4.72	4.73	4.72	4.72	4.71	4.71	4.70	4.69	4.69	4.68	4.68
6	4.81	4.79	4.76	4.75	4.73	4.72	4.73	4.72	4.71	4.71	4.71	4.71	4.71	4.70	4.70	4.69	4.69
5.5	4.77	4.75	4.74	4.72	4.71	4.71	4.70	4.70	4.70	4.70	4.70	4.70	4.70	4.70	4.70	4.69	4.69
5	4.71	4.70	4.70	4.70	4.68	4.69	4.69	4.68	4.69	4.69	4.69	4.69	4.69	4.69	4.69	4.69	4.69
4.5	4.68	4.66	4.67	4.67	4.67	4.66	4.67	4.68	4.68	4.68	4.69	4.69	4.69	4.70	4.70	4.70	4.70
4	4.65	4.64	4.65	4.65	4.65	4.66	4.66	4.66	4.67	4.67	4.68	4.69	4.69	4.70	4.70	4.71	4.72
3.5	4.64	4.64	4.63	4.63	4.64	4.64	4.65	4.65	4.66	4.66	4.67	4.68	4.69	4.69	4.70	4.70	4.71
3	4.62	4.63	4.63	4.62	4.63	4.63	4.63	4.64	4.65	4.66	4.66	4.67	4.68	4.69	4.69	4.70	4.71
2.5	4.62	4.62	4.62	4.62	4.62	4.62	4.63	4.63	4.64	4.65	4.65	4.66	4.67	4.68	4.69	4.70	4.72
2	4.62	4.61	4.61	4.62	4.62	4.62	4.62	4.63	4.63	4.64	4.65	4.66	4.66	4.67	4.69	4.70	4.71

x coordinate [mm]

Figure 12: Distribution of stress intensity factor (MPa$\sqrt{\text{m}}$)

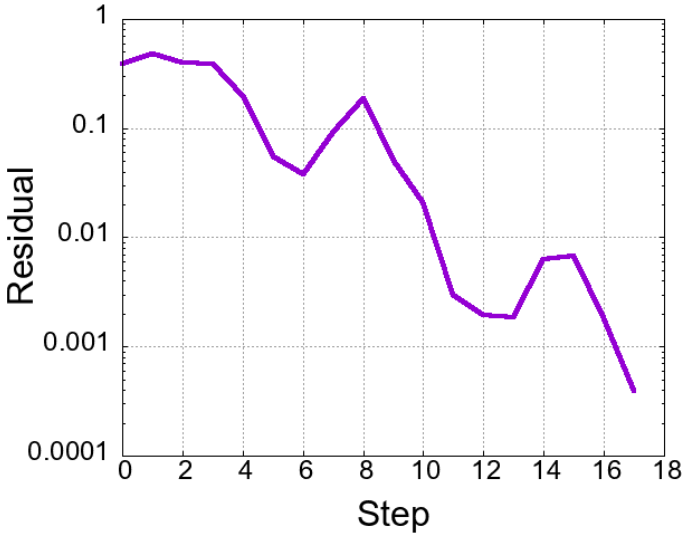

Figure 13: Residual history for hole center coordinates (1.75, 9)

3.4 Discussion

First, from Figure 10, the values of almost all maximum principal stresses are not reduced very much, indicating that an improperly placed hole increases the maximum principal stress. This could possibly make the die more fragile and prone to fatigue fracture. Conversely, the tendency of reduced maximum principal stress is clear. The coordinates (1.75, 9) are nearest the crack. Thus, as the coordinates of the hole center approach a crack, the maximum principal stress is reduced.

In the same way, from Figure 12, most of stress intensity factors are increased. Therefore, we concluded that an improperly placed hole also makes the die prone to brittle fracture. Accordingly, the stress intensity factor is the smallest at (1.75, 9). As the coordinates of the hole center approach the crack, the stress intensity factor is reduced.

Previous research [1] also showed a reduction of the tensile stress at the V-groove bottom by an appropriate hole. This study shows that a properly placed hole reduces the maximum principal stress and the stress intensity factor, which in turn reduces the potential for fatigue fracture and brittle fracture.

4 CONCLUSIONS

In this study, we evaluated fatigue and brittle modes using the maximum principal stress and stress intensity factor as evaluation indices.

A parametric analysis showed that a properly positioned hole in a V-bending die reduced the maximum principal stress and stress intensity factor.

By separating the meshes for the entire V-bending die and the hole to use coupling-matrix-free iterative s-version FEM, we realized hole relocation without remeshing. In conventional FEM, we must consider the difference in the shapes of meshes. In the method used here, the same meshes are used for the analysis, so we did not have to account for the difference in meshes. Additionally, we could make a script that easily performed the parametric study by without remeshing. Hence, the method in this study allowed us to do parametric analyses for a

structure with a hole automatically.

Regarding future work, although the only parameters of this analysis was the coordinates of the hole center, we need to perform the analysis with additional parameters, such as the hole shape and size. In addition, a parametric analysis with many degrees of freedom, such as the analysis in this study, takes a lot of computional time. We are going to consider a solution for this problem based on mathematical optimization.

ACKNOWLEDGMENTS

The authors greatly appreciate Prof. Takashi Kuboki for helpful advices and Mr. Yusuke Ueda for providing data for the bending process simulation. The present study was supported by The Amada Foundation and the Japan Society for the Promotion of Science, KAKENHI Grant Number JP19K14871.

REFERENCES

[1] Miyagawa, N. Design of V-bending die for plates to aim at life improvement (in Japanese). Graduation Thesis, University of Electro-Communications (2020).

[2] Yumoto, Y., Yusa, Y., Okada, H. An s-version finite element method without generation of coupling stiffness matrix by using iterative technique. *Mechanical Engineering Journal* (2016) **3**(5):16-00001.

[3] Fish, J. The s-version of the finite element method. *Computers & Structures* (1992) **43**(3):539-547.

[4] Yusa, Y., Okada, H., Yumoto, Y. Three-dimensional elastic analysis of a structure with holes using accelerated coupling-matrix-free iterative s-version FEM. International *Journal of Computational Methods* (2018) **15**(5):1850036.

[5] Okada, H., Higashi, M., Kikuchi, M., Fukui, Y., Kumazawa, N. Three dimensional virtual crack closure-integral method (VCCM) with skewed and non-symmetric mesh arrangement at the crack front. *Engineering Fracture Mechanics* (2005) **72**(11):1717-1737.

[6] Rybicki, E., Kanninen, M. F. A finite element calculations of stress intensity factors by a modified crack closure integral. *Engineering Fracture Mechanics* (1977) 9:931-938.

[7] Kobayashi, H. *Fracture mechanics* (in Japanese). Kyoritsu Shuppan CO., LTD. (1993).

[8] AMADA CO.,LTD. Bending mold list: HG-ATC die (V-bending die with 10-mm V-groove width). https://www.ai-link.ne.jp/free/products/kanagata/products/hg_atc_d/v10.html

[9] Ueda, Y. Shape optimization for V-bending die to avoid overload fracture (in Japanese). Graduation Thesis, University of Electro-Communications (2021).